Simulation of Rotating Continuous Casting of Steel: Thermo-hydrodynamics and Particles Motion

Grégory Fidel, Michel Bellet, Sylvain Witzke, Georges Martinez, Jérôme Giusti

Simulation of Rotating Continuous Casting of Steel: Thermo-hydrodynamics and Particles Motion

Grégory FIDEL[†♯] *, Michel BELLET[†], Sylvain WITZKE[♯], Georges MARTINEZ[♯], Jérome GIUSTI[♯]

[†] MINES ParisTech, CEMEF, UFR CNRS 7635, Sophia Antipolis, France
[♯] APERAM IMPHY, Imphy, France

Abstract

In Rotating Continuous Casting (RCC), the vertical billet, the mould and the support rolls rotate at about 1 rotation/sec. The mould is fed by a liquid steel free plunging jet. A numerical modelling of the RCC has been developed. The aim of this article is to study the effects of the free plunging jet and of the rotation on : the fluid flow, the thermal state, the solidification and on the particles motion. The modelling of the RCC uses a levelset method to capture the interface between the liquid steel and argon. A stabilized Navier-Stokes method is used to compute the fluid flow. A stabilized thermal solver is used to study the thermal field and the solidification of steel. A Euler-Lagrange approach is used to solve the motion of argon bubbles and inclusions. Hydrodynamics and particles motion are confronted to observations made on a cold water model. All developed methods are validated and applied to the RCC.

Keywords : Continuous casting ; plunging jet ; hydrodynamics ; heat-transfert ; solidification ; particles motion

1 Introduction

The Rotating Continuous Casting (RCC) of APERAM IMPHY (France) has two particularities : the vertical billet, the mould and the support rolls rotate at about 1 rotation/sec, and the mould is fed by a liquid steel free plunging jet, which passes through an argon protective atmosphere. When this jet impacts the liquid steel surface, it creates argon bubbles that are convected by fluid flow and can be captured by the solidification front (Fig. 1). The motion of particles in the RCC is significant for the surface quality of the billet. All these particularities affect especially the mold zone. Therefore the study is only focused on the primary cooling of the RCC.
A research work has been engaged in order to model the RCC including all its particularities. *Thercast*© is a 3D FE software, developed by CEMEF and TRANSVALOR, to model casting processes. The aim of this research is to enhance *Thercast*© to include the thermomechanicals effects of the free plunging jet and of the rotation. In parallel, APERAM Imphy has been built a Cold Water Model that allows visualizing the fluid flow. The aim of this article is to study the effects of the plunging jet and of the rotation on fluid flow, on particles motion and on solidification.The study is performed by observations on the cold water model of RCC and also by numerical modelling.
Firstly, the numerical modelling is described especially the levelset method for interface capturing. The stabilized Navier-Stokes formulation and the thermal resolution are briefly presented. Then the particle tracking is presented. Secondly, the experimental device and the physical modelling conditions are described. Finally, results are discussed.

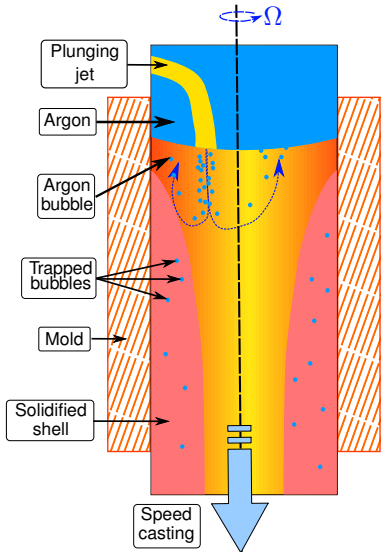

Fig. 1 – Rotating Continuous Casting

2 Theory

The modelling of RCC and of the cold water model are carried out using 3D finite elements. To apply this modelling to a free plunging jet in rotating fluid flow, it is necessary to capture the interface between the gas and the fluid, to compute the fluid flow and the thermal field. The method used to capture interface is a levelset method. The fluid flow is computed by using stabilized Navier-Stokes equations and the thermal problem is solved

* Corresponding author. Tel +33 (0)4 93 67 89 07; fax +33 (0)4 92 38 97 52. E-mail adress : gregory.fidel@mines-paristech.fr

by a temperature method with an equivalent specific heat.

2.1 Capturing interface

Let Γ_{ij} be the interface between a domain i and a domain j. Let $d(\Gamma_{ij}, x)$ be the distance function of a point x to the interface Γ_{ij}. The signed distance function is defined by :

$$\alpha(x) = \begin{cases} d\left(\Gamma_{ij}, x\right) & \text{if } x \in \Omega_i \\ 0 & \text{if } x \in \Gamma_{ij} \\ -d\left(\Gamma_{ij}, x\right) & \text{if } x \in \Omega - \Omega_i \end{cases} \quad (1)$$

With Ω_i the domain of the phase i, and Ω the whole domain (Fig. 2). All the notations are explained in the table at the end of the article. This function allows distinguishing

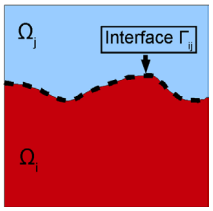

Fig. 2 – Multiphased domain

the interface between liquid steel and argon. This function is convected by a velocity field, $\boldsymbol{v}$, that is the solution of Navier-Stokes equations. A convective reinitialization method is used (see [VILLE et al., 2010] for details)

$$\begin{cases} \dfrac{\partial \alpha(x)}{\partial t} + (\boldsymbol{v} + \lambda \boldsymbol{U}) \nabla \alpha(x) = \lambda s(\alpha) \sqrt{1 - \left(\dfrac{\pi}{2E} \alpha(x)\right)^2} \\ \alpha(t=0, x) = \alpha_0 \end{cases} \quad (2)$$

Let λ be a parameter defined as : $\lambda = d\tau/dt$. s is the signed function defined as :

$$s(\alpha) = \begin{cases} -1 & \text{if } \alpha < 0 \\ 0 & \text{if } \alpha = 0 \\ 1 & \text{if } \alpha > 0 \end{cases} \quad (3)$$

2.1.1 Mixing properties

The levelset function allows mixing properties of the multiphase problem. A mixing law makes a transition between the different phases. This step is important because of huge differences between the phases. For example, between metal and argon, the density of metal is $\rho_m = 7000\ kg/m^3$ and the density of argon is $\rho_a = 1\ kg/m^3$. The mix law $M(x)$ used in our simulation is based on the volume fraction of each phase, which is estimated as :

$$M(x) = \frac{\sum_{i=0}^{N_n} \alpha(x_i) - \left| \sum_{i=0}^{N_n} \alpha(x_i) \right|}{2 \sum_{i=0}^{N_n} \alpha(x_i)} \quad (4)$$

N_n is the number of nodes per simplex. The mixed density and viscosity on the whole domain are defined by :

$$\rho = M(x)\rho_i + (1 - M(x))\rho_j \quad (5)$$

$$\eta = M(x)\eta_i + (1 - M(x))\eta_j \quad (6)$$

2.2 Hydrodynamics

To model fluid flow, Navier-Stokes incompressible equations in rotational frame are solved for velocity and pressure :

$$\begin{aligned} &\rho \left(\frac{\partial \boldsymbol{v}}{\partial t} + (\nabla \boldsymbol{v})\, \boldsymbol{v} \right) - \nabla \cdot (2\eta \nabla(\boldsymbol{v})) + \boldsymbol{\nabla} P = \\ &\rho \boldsymbol{g} - \underbrace{2\boldsymbol{\Omega} \times \boldsymbol{v}}_{\text{Coriolis force}} - \underbrace{\boldsymbol{\Omega} \times (\boldsymbol{\Omega} \times \boldsymbol{r})}_{\text{centrifugal force}} \\ &\nabla \cdot \boldsymbol{v} = 0 \end{aligned} \quad (7)$$

Due to the low viscosity of the liquid, to the free plunging jet and to the rotation, this is a high Reynolds number problem which requires a stabilized formulation (Variational MultiScale approach). This method has been developed in [HACHEM et al., 2010b]. For more details, the reader can refer to the previous reference.

2.3 Thermal problem

The thermal problem is solved for temperature in the framework of an enthalpic formulation to treat phase change.

$$\rho c_{\text{eq}} \left(\frac{\partial T}{\partial t} + \boldsymbol{v} \cdot \nabla T \right) - \nabla \cdot (k \nabla T) = 0 \quad (8)$$

In the heat equation, an equivalent specific heat is defined as follows :

$$c_{\text{eq}} = \frac{dH}{dT} = c_p + L \frac{df_l(T)}{dT} \quad (9)$$

Where the liquid fraction is defined a priori as a function of temperature. The stabilization methods SCPG and SUPG have been used :
[HACHEM, 2009],[HACHEM et al., 2010a] for more details.

2.4 Particles motion

The surface quality of the billet is highly depending on the inclusionary cleanliness. Besides, due to free plunging jet feeding the RCC, a lot of bubbles are generated and they can be captured by the solidification front. The modelling of the motion of these particles (argon bubble and inclusion) allows to better understanding how to decrease the number of captured particles. The particles are considered as rigid spheres. Their grow up, rupture and coalescence are not included. The motion of the particles

is integrated by using a Euler-Lagrange approach : the fluid id considered as a continuous phase governed by Navier-Stokes equations whereas the particles are viewed as a discrete phase governed by the second Newton's law. This approach is valid when the particles density is low enough to neglect their influence on the fluid flow. The Euler-Lagrange approach has been successfully used to calculate the particle motion in continuous casting by [PFEILER et al., 2007], [YUAN and THOMAS, 2006] and [ZHANG et al., 2004]. The equilibrium equation for particles is :

$$\begin{aligned} \frac{d\boldsymbol{x}_p}{dt} &= \boldsymbol{v}_p \\ m\frac{d\boldsymbol{v}_p}{dt} &= \boldsymbol{F}_D + \boldsymbol{F}_L + \boldsymbol{F}_{\text{Pres}} + \boldsymbol{F}_{\text{Stres}} + \boldsymbol{F}_A + \boldsymbol{F}_G \end{aligned} \tag{10}$$

Where the terms on the right hand side in equation (10) are : steady-state drag force, lift force due to the velocity gradient, pressure gradient force and stress gradient force, added mass force arising from the acceleration of the surrounding fluid, gravitational force that includes the gravitational effect and the buoyancy effect. Expressing the different forces, it can be shown that the particles motion is driven by the equation below. ([YUAN, 2004], [CROWE et al., 1998])

$$\begin{aligned} &\left(1+\frac{C_a\rho}{2\rho_p}\right)\frac{d\boldsymbol{v}_p}{dt} = \frac{1+0.15Re_p^{0.687}}{\tau_v}(\boldsymbol{v}-\boldsymbol{v}_p) \\ &+0.07568J\frac{d_p}{\tau_v\sqrt{\eta/\rho|\nabla\times\boldsymbol{v}|}}\left[(\boldsymbol{v}-\boldsymbol{v}_p)\times(\nabla\times\boldsymbol{v})\right] \\ &+\left(1+\frac{Ca}{2}\right)\frac{\rho}{\rho_p}\frac{D\boldsymbol{v}}{Dt}+\boldsymbol{g}\left(1-\frac{\rho}{\rho_p}\right) \end{aligned} \tag{11}$$

With $D\boldsymbol{v}/Dt = \frac{\partial \boldsymbol{v}}{\partial t} + (\boldsymbol{v}\cdot\nabla)\boldsymbol{v}$. The particle velocity response time is defined as $\tau_v = \rho_p {d_p}^2/18\eta$. J is defined as :

$$\begin{aligned} J =& 06765[1+tanh(2.5log_{10}\epsilon+0.191)] \\ & [0.667+tanh(6(\epsilon-0.32))] \end{aligned} \tag{12}$$

Where $\epsilon = \sqrt{Re_G}/Re_p$, $Re_p = \rho|\boldsymbol{v}-\boldsymbol{v}_p|d_p/\eta$ and $Re_G = \rho G d_p^2/\eta$. G is the norm of the velocity gradient. The correction factor due to the acceleration effect C_A is defined as :

$$C_A = 2.1 - \frac{0.132}{0.12+A_c^2} \tag{13}$$

The acceleration parameter A_c is defined as :

$$Ac = \frac{|\boldsymbol{v}-\boldsymbol{v}_p|^2}{d_p\frac{d|\boldsymbol{v}-\boldsymbol{v}_p|}{dt}} \tag{14}$$

2.4.1 Numerical solving

Firstly, the fluid velocity field is calculated. This field is used to move particles. To solve equation (11), an explicit fourth order Runge-Kutta method is used.

$$\begin{cases} \boldsymbol{x}_n \\ \boldsymbol{K}_1 = \Delta t\cdot\dfrac{d\boldsymbol{v}_p}{dt}(\boldsymbol{x}_n, t_n) \\ \boldsymbol{K}_2 = \Delta t\cdot\dfrac{d\boldsymbol{v}_p}{dt}\left(\boldsymbol{x}_n+\dfrac{\boldsymbol{K}_1}{2}, t_n+\dfrac{\Delta t}{2}\right) \\ \boldsymbol{K}_3 = \Delta t\cdot\dfrac{d\boldsymbol{v}_p}{dt}\left(\boldsymbol{x}_n+\dfrac{\boldsymbol{K}_2}{2}, t_n+\dfrac{\Delta t}{2}\right) \\ \boldsymbol{K}_4 = \Delta t\cdot\dfrac{d\boldsymbol{v}_p}{dt}(\boldsymbol{x}_n+\boldsymbol{K}_3, t_n+\Delta t) \\ \boldsymbol{x}_{n+1} = \boldsymbol{x}_n + \dfrac{1}{6}(\boldsymbol{K}_1+2(\boldsymbol{K}_2+\boldsymbol{K}_3)+\boldsymbol{K}_4) \end{cases} \tag{15}$$

At each iteration, the speed of each particle is constant. That means, in equation (11), $\boldsymbol{v} = (\boldsymbol{x}, t)$ and $\boldsymbol{v}_p = \boldsymbol{v}_p(\boldsymbol{x}_n, t)$. If the time step for the particles is smaller than the time step of the fluid, some sub-increments are solved. In this case, the fluid flow is assumed to be stationary.

2.5 Solution algorithm

To conclude this section, the general algorithm that has been developed to model the RCC is explained on Fig. 3. The interface between argon and steel is captured by a

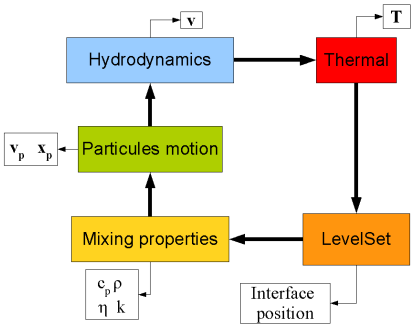

Fig. 3 – Numerical algorithm

convective reinitialization method. The fluid flow is solved using a stabilized Navier-Stokes method. The thermal problem is solved by using an equivalent specific heat. That allows having the effect of the free plunging jet on the fluid flow and on the thermal field. The particles are tracked by a Euler-Lagrange method. All the modelling is carried out with the scientific library *CimLib* developed at *CEMEF*.

3 Experimental device and conditions of simulation

3.1 The Cold Water Model (CWM)

The cold water model of RCC (CWM) is built to study hydrodynamics phenomena appearing in the RCC. It also serves to validate the hydrodynamic modelling. Fig.4

shows the experimental device. Water falls down from the tundish (Fig. 4(a)) through the nozzle (Fig. 4(b)) in a transparent plastic tube which represents the mold of the RCC (Fig. 4(c)). This tube is rotated by an engine (Fig. 4(b)). The water exits from a flood gate placed at the bottom of the tube. Then the water is pumped back to the tundish (Fig. 4(d)). A digital camera is used to provide

(a) Tundish

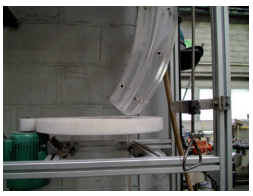

(b) Nozzle and rotating system

(c) Mold (d) Exit, water tank and pump

Fig. 4 – Cold Water Model

qualitative study of the fluid flow. Several positions and orientations of the jet were studied. The effect of the speed rotation is also investigated.

3.2 Modelling of Cold Water Model (CWM)

Only the mould and the air above are modelled. The rotation is represented by the speed boundary condition. The jet is modelled by a cylinder where the speed and the value of the levelset are imposed. All the boundary conditions are described on Fig. 5.

For the modelling, the following parameters are chosen : $\eta_a = 1 \cdot 10^{-4} Pa.s$, $\rho_a = 1\ kg/m^3$, $\eta_l = 1 \cdot 10^{-3}\ Pa.s$, $\rho_l = 1000\ kg/m^3$. The mesh is unstructured, of uniform size and isotropic. The mesh size is $h = 1\ cm$. The injection speed is imposed to $|\boldsymbol{V}_i| = 0.87 m/s$ and the exit speed is imposed to $|\boldsymbol{V}_c| = 0.14\ m/s$.

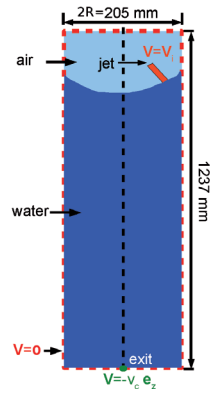

Fig. 5 – Boundary conditions

4 Results

4.1 Rotation & emptying

To validate the rotation of the fluid, the position of the interface is a good indicator. For a perfect (non-viscous) fluid, the analytical position of the interface is :

$$h(r) = h_0 + \frac{\|\boldsymbol{\Omega}\|^2}{4\|\boldsymbol{g}\|}\left(2r^2 - R^2\right) \tag{16}$$

A validation modelling is realized on a cylinder water tank ($R = 1\ m$, $H = 1\ m$ and $h_0 = 0.5\ m$) assuming sticky contact at the wall. Fig.6 shows the comparison between modelling and analytical solution for different rotation speeds. The analytical solution and the simulation give quite close results.

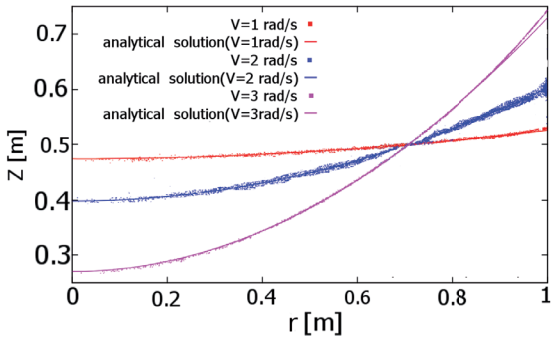

Fig. 6 – Effect of rotation speed on the free surface. Modelling vs analytical solution for three different speeds

When the CWM is emptying with rotation, but without free plunging jet, a vortex appears. This kind of fluid flow is known as Rankine's vortex. Indeed, in such a fluid flow, the position of the interface is ([GUYON et al., 2001]) :

$$h(r) = h_0 - \frac{\|\boldsymbol{\Gamma}\|^2}{8\pi^2\|\boldsymbol{g}\|r^2} \tag{17}$$

This solution is valid only far from the heart of the vortex. Fig.7 shows this phenomenon. Fig. 8 compares modelling with the observation and the analytical solution. Two series of experimental measurement are given corresponding to

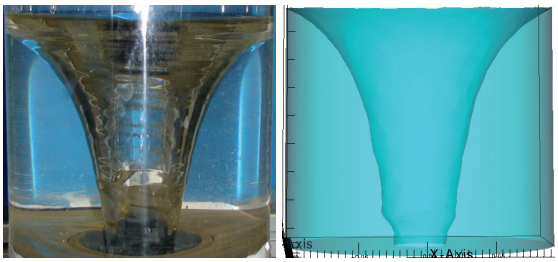

(a) Experiment (b) Modeling

Fig. 7 – Rankine's vortex formed when emptying the rotating water model

the "left" and "right" side on Fig. 7(a). Error bars due to pixelisation are given. There is a good agreement between

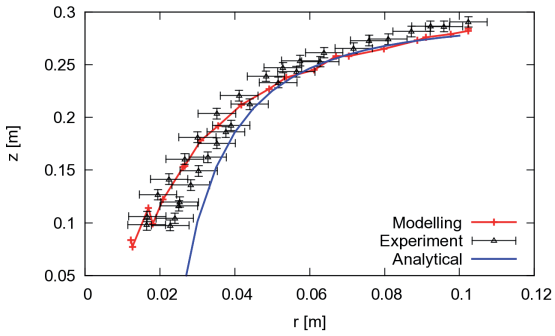

Fig. 8 – Comparison between analytical solution, modelling and experiment

the modelling, the experiment and the analytical solution far from the heart of the vortex. As expected, both the experimental and the calculated profiles depart from the analytical one for the lower z.

4.2 Free plunging jet

The observation of CWM provides a good illustration of the major effects of the position of the jet on fluid flow. Indeed,

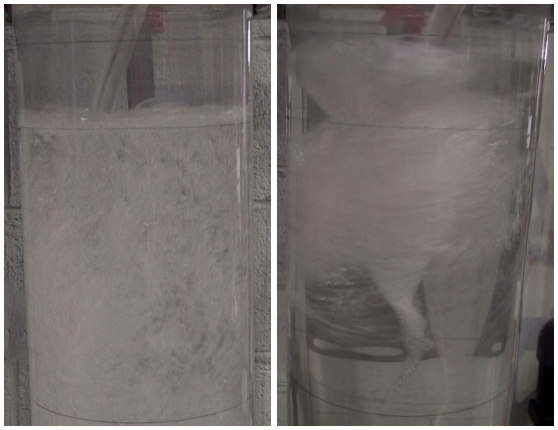

(a) counter rotational jet (b) co-rotational jet

Fig. 9 – Effect of the orientation of the jet onto the fluid flow

when the jet arrives in the opposite way with respect to rotation, the flow is quite quiet (Fig. 9(a)). Conversely, if the jet arrives in the same way as the rotation (Fig. 9(b)), the flow is very disturbed. The jet speeds up the flow in the surface area. Moreover, the jet slows down the upstream liquid with respect to the jet. The fluid circles the jet and plunges. This effect is shown on Fig. 10. Shown in Fig. 9 and Fig. 10, a lot of bubbles are generated by the plunging jet. However in the RCC, less bubbles are generated.

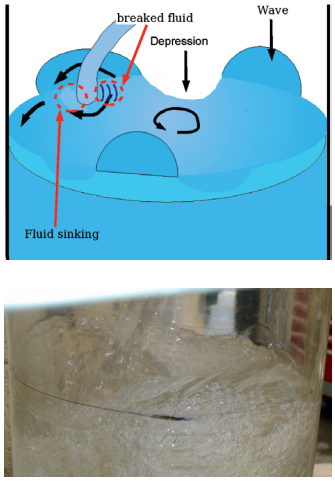

Fig. 10 – Effect of the jet in opposite way

There is no measure of fluid speed on the CWM. The only indicator that can be extracted is the shape of the meniscus which can be used for validation. As can be seen from Fig. 11(a), the meniscus, in the counter way case, is nearly parabolic. So the jet weakly disturbs the interface. When injecting in the same way as rotation (Fig. 11(b)), the surface is very disturbed. So qualitatively, the modelling gives similar results compared to the experiment on the cold water model.

(a) counter rotational (b) co-rotational

Fig. 11 – Modelling of the free plunging jet in a rotating CWM

The rotation speed also affects the surface. The higher the speed, the more disturbed the surface is. The comparison between observations (Fig. 12) and modelling (Fig. 13) shows a good agreement.

(a) $\Omega = 0.5$ rot$/s$

(b) $\Omega = 1$ rot$/s$

(c) $\Omega = 1.5$ rot$/s$

Fig. 12 – Effect of the rotation speed on the free surface shape (experiment)

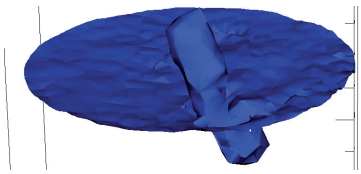

(a) $\Omega = 0.5$ rot$/s$

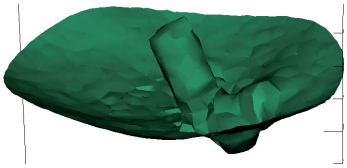

(b) $\Omega = 1$ rot$/s$

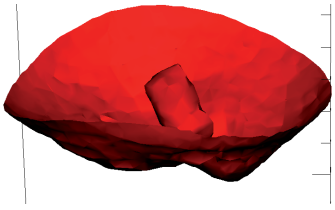

(c) $\Omega = 1.5$ rot$/s$

Fig. 13 – Effect of the rotation speed on the free surface shape (modelling)

4.3 Thermo-hydrodynamics

In this section, the thermo-hydrodynamics problem of the RCC is studied, especially the position of the jet which is known to affect the thermal field and the solidification. The boundary conditions of the RCC's modelling are summarized on Fig. 14. The following parameters are

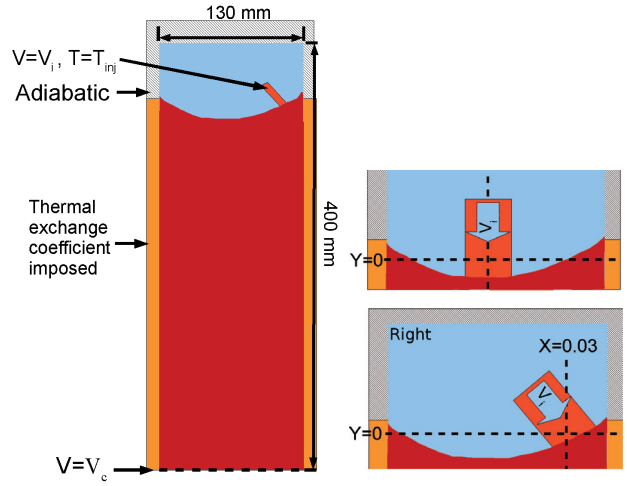

(a) Thermomechanics boundary conditions (b) Jet position

Fig. 14 – Boundary conditions

chosen : $\boldsymbol{v}_c = 0.025\ m/s$, $\boldsymbol{v}_i = 0.1725\ m/s$. The position, the speed and the orientation of the jet is imposed. The temperature of the jet is imposed to $T_{inj} = 1500^{\circ}C$. The exchange between the mold and the steel is : $\Phi = h(T - T_{ext})$ with $h = 1000\ W/m^2$ and $T_{ext} = 30^{\circ}C$. The solidus temperature is $T_s = 1308^{\circ}C$ and the liquidus temperature is $T_l = 1461^{\circ}C$.

The effects of the position of the jet are studied in a 2D plane case. So the effect of the rotation is not included. The modelling used an unstationary Eulerian approach with a fixed domain. The modelling needs to reach a quasi-stationary state before the results are usable. Fig. 15 gives the evolution of the temperature and the solid fraction for a point located at $x = 0.06\ m$ and $z = 0.34\ m$. The quasi-stationary state is reach about 25s.

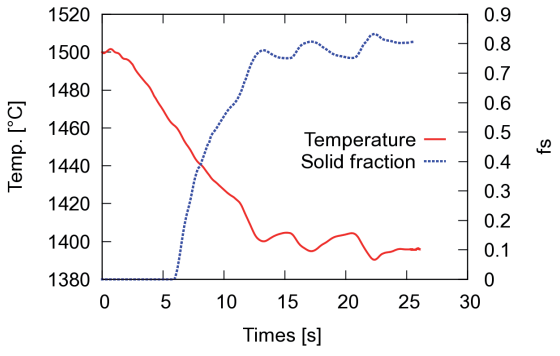

Fig. 15 – Evolution of temperature and solidification to the quasi-stationary state

The effect of the position of the jet on the thermal field is visible on Fig. 16. The jet is put on the left side near the

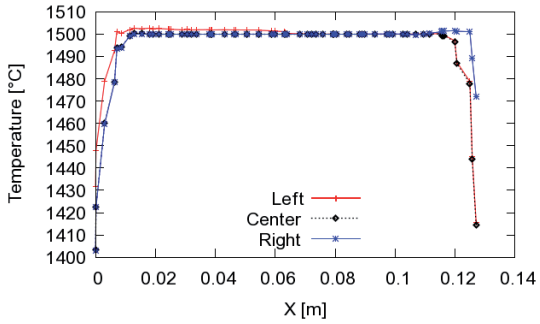

Fig. 16 – Effects of the position of the jet on the thermal field

mold, on the center of the mold and on the right side near the mold. If the jet arrives from the left (red curve) there is a superheat located on the left. On the other side, the superheat is located on the right.
Fig. 17 shows the velocity distribution. Velocity vectors are in black and the color is the speed magnitude. The gas /metal interface is represented by the thick line. The position of the jet affects this distribution. When the jet is at the center position (Fig. 17(a)), several recirculations are visible. The fluid flow is non-symmetric. When the jet is on the right (Fig. 17(b)), the liquid metal sticks to the border before it creates a recirculation.

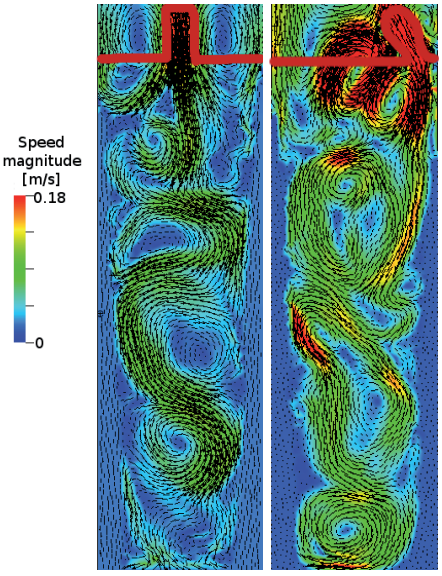

(a) Center (b) Right

Fig. 17 – Velocity field : effect of the jet's position ($t = 30\ s$)

Fig. 18 shows the distribution of the superheat affected by the jet's position. Only the metal is visible. When the jet is at the center (Fig. 18(a)), several recirculations are visible. When the jet is on the right side (Fig. 18(b)), it seems that a more marked recirculation in the upper zone of the mold contributes to an earlier elimination of the superheat (resulting in lower liquid temperature in the lower zone).

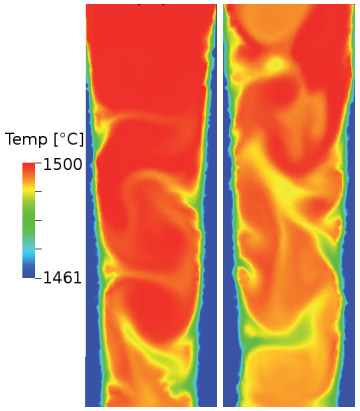

(a) Center (b) Right

Fig. 18 – Distribution of the superheat : effect of the jet's position

Fig. 19 shows the solidified fraction. If the jet is at the center (Fig. 19(a)), the solidified shell, in red, grows steadily and symmetrically. But if the jet is on the right (Fig. 19(b)), the solidified shell is asymmetric. Indeed the impact zone of the jet is always warmed up by the jet.

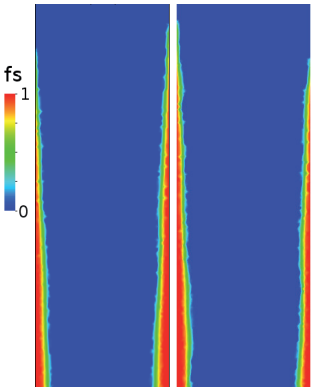

(a) jet at the center (b) jet on the right

Fig. 19 – Solid fraction : effect of the jet's position

In Fig. 20, the solidified shell thickness over the distance from the meniscus is represented.

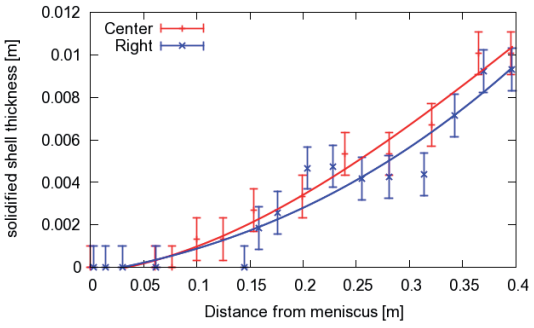

Fig. 20 – Solidified shell thickness : effects of the jet position

In both case the shell thickness at the exit of the mold is above 1 cm. This a common value for this size of billet. When jet is on the right, the solidification of steel start deeper.

4.4 Particles motion

In a rotating flow, it can be expected that particle tracking requires a good time integration scheme in order to avoid artificial centrifugal motion. To evaluate this effect, particles motion is modelled in a Couette flow. The rotation speed is $\vec{\Omega} = 1\ rad/s$. The fluid is water : $\rho = 1000\ kg/m^3$, $\eta = 1 \cdot 10^{-3}\ Pa \cdot s$. Three types of particles are studied :
– fluid particle : $\rho_p = 1000\ kg/m^3$
– light particle : $\rho_p = 1\ kg/m^3$
– heavy particle : $\rho_p = 1300\ kg/m^3$
All the particles have the same radius $r_p = 1\ mm$. Fig .21 illustrates the particles migration due to the rotation of the fluid. As expected, the fluid particle trajectory is a circle

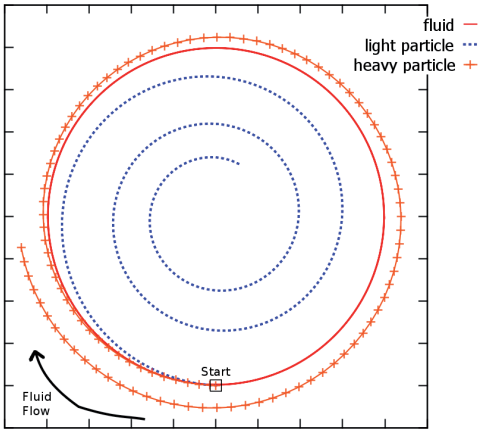

Fig. 21 – Particles motion in Couette flow

and thus no numerical artefact affects the trajectory of the fluid. Also, the light particle migrates to the center while the heavy particle is ejected to the periphery.
The analysis of the forces magnitude shows that the shear lift force (second term of the right member of the equation (10)) is negligible in comparison with the other forces. The migration to the center of the light particles is visible only if the effect of the stress gradient is included in the equation (10). Several rotation speeds have been tested in the Couette's flow (Fig. 22). The analysis of the forces shows that the higher the speed rotation , the higher the drag forces. It is the same for the stress gradient force and the added mass force. The drag force always dominates the other forces.
In a quiescient environment ($\boldsymbol{v} = 0$), the ultimate velocity of a particle is known analytically for two simple cases :
– Surface tension dominant ([STOKES, 1880]) : $v_\infty = \frac{\boldsymbol{g} d_p^2 (\rho - \rho_p)}{18\eta}$
– Large bubble ([DAVIES and TAYLOR, 1985]) : $v_\infty = 0.707\sqrt{\boldsymbol{g} d_p}$

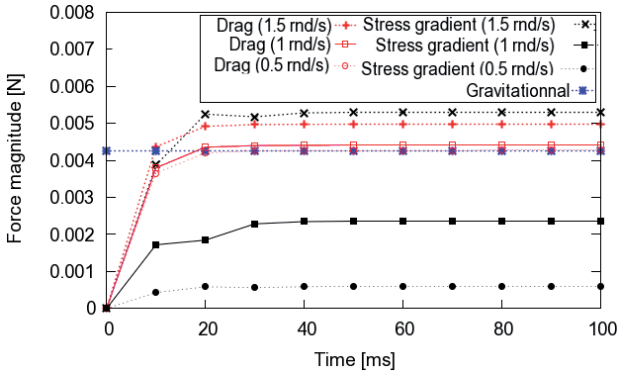

Fig. 22 – Forces acting on a bubble in Couette flow

Fig.23 shows the terminal velocity for several bubbles diameter that pass through the surface dominant case to large bubble case. When the bubbles are small enough,

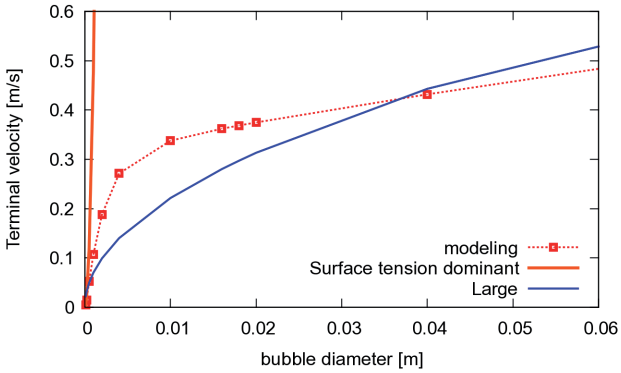

Fig. 23 – Terminal velocity of an air bubble in a quiescent water

the terminal velocity of bubbles correspond to the surface tension dominant case. When the bubbles are large the terminal velocity is closed to the large bubbles case. Between these two cases, the terminal velocity is far from the two solutions.
To explore the particles motion in the CWM, polymer particles are dropped in the rotating fluid flow with the free plunging jet . Two types of particles are used : the lighter particles are made of HDPA ($\rho_p = 900\ kg/m^3$) and the heaviest are made of PMMA ($\rho_h = 1100\ kg/m^3$). The particles are spherical with a radius $r_p = 1\ mm$. The lighter particles float a long time near the surface while they rotate but the heavier sink down directly to the bottom of the CWM during the rotation. A modelling of these experiments were also realized with the same properties. The trajectory of the lightest particle (plain line on Fig. 24) illustrate that it directly goes to the surface. Conversely, the heaviest particle sink during rotation (dashed lines on Fig. 24). The interface between the air and the fluid is visible in grey.
With this validation, the particles motion can be studied in the RCC. According to [ZHANG and TANIGUCHI, 2004] bubble size is in the range $5\ -\ 20\ mm$ in the case of

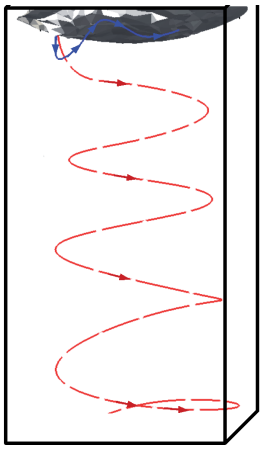

Fig. 24 – Particles motion in CWM

continuous casting. The injection zone is located under the impact point of the jet. The particles are continuously injected in the metal. In this example, the transport of argon bubbles and alumina inclusions is studied. Argon bubbles are particles with following properties : $\rho_p = 1kg/m^3$ and a fixed radius $r_p = 0.005m$. Alumina inclusions are particles with following properties : $\rho_p = 2700kg/m^3$ and $r_p = 100\mu m$. In Fig. 25 the interface between the argon and the metal is the black line. The color represents the solid fraction (red : solid, white liquid). This allows to say that inclusions go deeper and faster in the liquid than bubbles. Also the bubbles are captured by the solidified acoording to a rough criterion. Indeed, when the bubble is found in teh mushy zone below a critical liquid fraction, capture is declared ($v_p = v_c$).

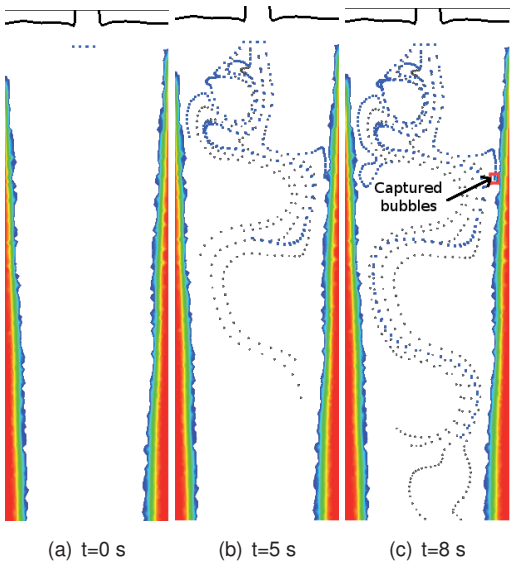

Fig. 25 – Particles motion in RCC : argon bubble (blue dot) and alumina inclusion (grey dot)

Fig. 26 shows the trajectory of three bubbles of different radius in the case of the jet located at the center. The bigger bubble (red line) goes up to the surface of the steel (black dash line). The smaller bubble (blue line) went down deeply in the liquid steel. The middle size bubble (black line) evolves near the surface. Also the bigger the bubbles, the deeper they go.

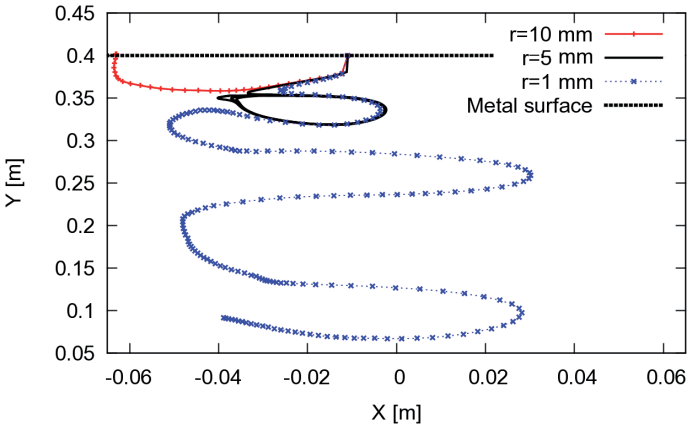

Fig. 26 – Trajectories of different size bubbles

5 Conclusions and perspectives

In order to understand the effects of the free plunging jet and the effect of the rotation on the fluid flow, on the particles flow and on the solidification in the RCC, experiment on a cold water model and a 3D finite element modelling are realized. New tool has been developed in order to include all the particularities of the RCC. The modelling uses a levelset method to track the interface between metal and argon. A stabilized Navier-Stokes formulation is used to compute the fluid flow in the RCC. The hydrodynamics of the RCC was compared between the observation on the CWM, the modelling and some analytical results. This study shows the great effects of the position and the orientation of the jet on the surface of the liquid and also on the fluid flow. Heat-transfer in RCC has been studied. The effects of the position of the jet on the solidification and on the thermal field are studied. The modelling has shown that the asymmetric caused by the jet can significantly affect the growth of solidified shell. The particles motion has been modelled by using an Euler-Lagrange approach. The bubbles motion has been studied in the case of the CWM. The bubbles and inclusions motion are studied in the case of the RCC. In this case, the bigger the bubbles, the deeper they go. The inclusions go faster and deeper than argon bubbles. Now it's possible to model the RCC including : the fluid flow, the free plunging jet, the solidification and the particle motion. This work is the first-step development in the modelling of the RCC. At the end, this model will couple the hydrodynamics with solid mechanics. This new method allows modelling the thermomechanical state of the solidified shell including the effects of the free plunging

and the rotation. This should be a efficient tool to speedup the development of new steel grade , improve the processing conditions and the quality of the product.

c_{eq}	equivalent specific heat	$J/kg/K$
c_p	specific heat	$J/kg/K$
d	diameter	m
$d(\Gamma_{ij}, x)$	distance function of a point x from the interface Γ_{ij}	m
f_l	liquid fraction	$-$
f_s	solid fraction	$-$
$\boldsymbol{g}$	gravity vector	m/s^2
$h(r)$	water level	m
h_o	initial water level	m
L	latent heat	J/kg
$M(x)$	Mixing law	$-$
P	pression	Pa
r	radial position	m
R	radius	m
Re	Reynolds number	$-$
t	time	s
$\boldsymbol{U}$	reinitializing speed of levelset	
$\boldsymbol{v}$	velocity vector	m/s
α	levelset function	m
η	dynamic viscosity	$Pa \cdot s$
Γ_{ij}	interface between a phase i and a phase j	$-$
$\vec{\Gamma}$	vorticity	m^2/s
Ω	rotation speed	rad/s
ρ	density	kg/m^3
RCC	Rotating Continuous Casting	$-$
CWM	Cold Water Model	$-$
$_p$	relative to the particles	$-$

TABLE 1 – Notation

References

[CROWE et al., 1998] CROWE, C., SOMMERFILD, M., and TSINJI, Y. (1998). *Multiphase Flows with Droplets and Particles*. CRC Press.

[DAVIES and TAYLOR, 1985] DAVIES, R. M. and TAYLOR, G. (1985). The mechanics of large bubbles rising through extended liquids and through liquids in tubes. In *Proceedings of the Royal Society of London. Series A, Mathematical and Physical Sciences*, volume 200, pages 375–390. The Royal Society.

[GUYON et al., 2001] GUYON, E., HULIN, J.-P., and PETIT, L. (2001). *Hydrodyanmique Physique*. EDP Science.

[HACHEM, 2009] HACHEM, E. (2009). *Stabilized Finite Element Method for Heat Transfer and Turbulent Flows inside Industrial Furnaces*. PhD thesis, MinesParistech.

[HACHEM et al., 2010a] HACHEM, E., DIGONNET, E., KOSSEIFI, N., MASSONI, E., and COUPEZ, T. (2010a). Enriched finite element spaces for transient conduction heat transfer. *Applied Mathematics and Computation*, 217(8) :3929 – 3943.

[HACHEM et al., 2010b] HACHEM, E., RIVAUX, B., KLOCZKO, T., DIGONNET, H., and COUPEZ, T. (2010b). Stabilized finite element method for incompressible flows with high reynolds number. *Journal of Computational Physics*, 229(23) :8643 – 8665.

[PFEILER et al., 2007] PFEILER, C., WU, M., LUDWIG, A., and THOMAS, B. (2007). Particle entrapment in the mushy region of a steel continuous caster. In *SteelSim 2007*, pages 247–252.

[STOKES, 1880] STOKES, G. G. (1880). *Mathematical and physical*, volume 1. Cambridge University Press.

[VILLE et al., 2010] VILLE, L., SILVA, L., and COUPEZ, T. (2010). Convected level set method for the numerical simulation of fluid buckling. *International Journal for Numerical Methods in Fluids (in press)*.

[YUAN, 2004] YUAN, Q. (2004). *Transient study of turbulent flow and particle transport during continuous casting of steel slabs*. PhD thesis, University of Illinois at Urbana-Champaign.

[YUAN and THOMAS, 2006] YUAN, Q. and THOMAS, B. G. (2006). Transport and entrapement of particles in continuous casting of steel. In TMS, editor, *Modeling of Casting, Welding and Advanced Solidification Processes-XI*, pages 745–752.

[ZHANG et al., 2004] ZHANG, L., J., A., and THOMAS, B. (2004). Inclusion removal by bubble flotation in continuous casting mold. In *Materials Science & Technology*, volume 2, pages 1045–1056, New Orleans.

[ZHANG and TANIGUCHI, 2004] ZHANG, L. and TANIGUCHI, S. (2004). Fundamentals of inclusions removal from liquid steel by bubbles flotation. *International Materials Reviews*, 45(2) :59–82.